

A WKB method based on parabolic cylinder function for very-low-frequency sound propagation in deep ocean

Jian-Kang Zhan(詹建康), Sheng-Chun Piao(朴胜春), Li-Jia Gong(龚李佳), Dong Yang(董阳), Yong-Chao Guo(郭永超), and Guang-Xue Zheng(郑广学)

Citation: Chin. Phys. B, 2025, 34 (**3**): 034301. DOI: 10.1088/1674-1056/ada886
Journal homepage: http://cpb.iphy.ac.cn; http://iopscience.iop.org/cpb

What follows is a list of articles you may be interested in

Energy-distributable waterborne acoustic launcher for directional sensing

Tian Yang(杨天), Wenting Gao(高文婷), Shida Fan(范世达), Jie Ren(任捷), and Tianzhi Yang(杨天智)
Chin. Phys. B, 2023, 32 (**12**): 124302. DOI: 10.1088/1674-1056/acf5cf

Fast estimation of distance between two hydrophones using ocean ambient noise in multi-ship scenarios

Xuefeng Liu(刘雪枫), Zhi Xia(夏峙), Qi Li(李琪), and Ye Ding(丁烨)
Chin. Phys. B, 2023, 32 (**12**): 124301. DOI: 10.1088/1674-1056/acf91b

Method for measuring the low-frequency sound power from a complex sound source based on sound-field correction in a non-anechoic tank

Hongzhe Xu(徐宏哲), Qi Li(李琪), Rui Tang(唐锐), and Dajing Shang(尚大晶)
Chin. Phys. B, 2023, 32 (**5**): 054303. DOI: 10.1088/1674-1056/acb75c

A passive source ranging method based on the frequency warping transform of the vertical intensity flux in shallow water

Yu-Bo Qi(戚聿波), Shi-Hong Zhou(周士弘), Meng-Xiao Yu(于梦枭), Shu-Yuan Du(杜淑媛), Mei Sun(孙梅), Ren-He Zhang(张仁和)
Chin. Phys. B, 2019, 28 (**5**): 054302. DOI: 10.1088/1674-1056/28/5/054302

Influence of warm eddies on sound propagation in the Gulf of Mexico

Yao Xiao(肖瑶), Zhenglin Li(李整林), Jun Li(李鋆), Jiaqi Liu(刘佳琪), Karim G Sabra
Chin. Phys. B, 2019, 28 (**5**): 054301. DOI: 10.1088/1674-1056/28/5/054301

A WKB method based on parabolic cylinder function for very-low-frequency sound propagation in deep ocean

Jian-Kang Zhan(詹建康)[1,2,3], Sheng-Chun Piao(朴胜春)[1,2,3,†], Li-Jia Gong(龚李佳)[1,2,3], Yang Dong(董阳)[1,2,3], Yong-Chao Guo(郭永超)[3], and Guang-Xue Zheng(郑广学)[3]

[1] *National Key Laboratory of Underwater Acoustic Technology, Harbin Engineering University, Harbin* 150001, *China*
[2] *Key Laboratory of Marine Information Acquisition and Security (Harbin Engineering University), Ministry of Industry and Information Technology, Harbin* 150001, *China*
[3] *College of Underwater Acoustic Engineering, Harbin Engineering University, Harbin* 150001, *China*

(Received 11 November 2024; revised manuscript received 6 January 2025; accepted manuscript online 10 January 2025)

A Wentzel–Kramers–Brillouin (WKB) method is introduced for obtaining a uniform asymptotic solution for underwater sound propagation at very low frequencies in deep ocean. The method utilizes a mode sum and employs the reference functions method to describe the solution to the depth-separated wave equation approximately using parabolic cylinder functions. The conditions for the validity of this approximation are also discussed. Furthermore, a formula that incorporates waveguide effects for the modal group velocity is derived, revealing that boundary effects at very low frequencies can have a significant impact on the propagation characteristics of even low-order normal modes. The present method not only offers improved accuracy compared to the classical WKB approximation and the uniform asymptotic approximation based on Airy functions, but also provides a wider range of depth applicability. Additionally, this method exhibits strong agreement with numerical methods and offers valuable physical insights. Finally, the method is applied to the study of very-low-frequency sound propagation in the South China Sea, leading to sound transmission loss predictions that closely align with experimental observations.

Keywords: WKB method, normal modes, very-low-frequency sound propagation, parabolic cylinder function

PACS: 43.30.+m, 43.30.–k

DOI: 10.1088/1674-1056/ada886 **CSTR:** 32038.14.CPB.ada886

1. Introduction

The theory of normal modes, which entails representing the sound field as a sum of orthogonal normal modes, has been a fundamental concept in the field of underwater acoustics for numerous years. Initially, Pekeris[1] developed a normal mode theory for sound propagation in shallow water, considering a waveguide with a pressure-release surface and a penetrable fluid bottom. Subsequently, Deavenport[2] derived an analytical expression for normal modes in an underwater acoustic duct with an Epstein layer. However, the availability of exact solutions is limited. The Wentzel–Kramers–Brillouin (WKB) approximation, also known as the WKBJ or LG approximation,[3–5] offers an asymptotic solution to the normal mode equation when the wavelength is significantly smaller than the spatial scale of medium variability.[6–9] Rooted in semiclassical physics,[10,11] this technique has been applied extensively in various contexts of acoustics and vibrations, providing a versatile framework for addressing complex wave propagation problems.[12–16]

The study of very-low-frequency (VLF) sound propagation in the deep ocean is essential for various applications, such as subsea geological exploration, submarine communication, and marine biology research.[17] VLF sound can travel long distances underwater with minimal energy loss and is affected less by changes in the marine environment, making it ideal for long-distance underwater communication. Our research is focused on applying the WKB method to ocean acoustics, specifically in the context of VLF sound propagation in the deep ocean. Budden[18] provided an eigenfunction based on the classical WKB approximation. Henrick *et al.*[19] then used the uniform WKB approach with boundary-layer corrections to approximate the normal modes at 100 Hz for an underwater sound channel. Zhang *et al.*[20] introduced a WKBZ mode method for analyzing pulse propagation in ocean channels, which was further utilized for computing the propagation of signal energy and waveform. Later, Ainslie *et al.*[21] introduced an approach based on the WKB approximation and the Tindle–Weston formula, specifically designed to solve the bottom-interacting field including leaky modes. Aksenov *et al.*[22] used the modal WKB approximation to analyze the distribution of sound pressure and phase gradient in the frequency range of 45 Hz–650 Hz in the deep sea along signal propagation paths. Additionally, the WKB approximation has been used widely to study the properties of VLF underwater sound

[†]Corresponding author. E-mail: piaoshengchun@hrbeu.edu.cn

© 2025 Chinese Physical Society and IOP Publishing Ltd. All rights, including for text and data mining, AI training, and similar technologies, are reserved.

fields, as demonstrated by Guthrie[23] and Beilis.[24]

In deep water, a multitude of normal modes are excited at high frequencies, leading to extensive computational requirements. To address this, Leibiger[25] developed the RAYMODE model by integrating normal mode theory with ray theory, offering an efficient solution for analyzing underwater sound fields. However, note that the WKB approximation may not provide accurate results at low frequencies in the range of 10 Hz–100 Hz for sound propagation in the ocean.

Previous studies of VLF sound propagation in the deep ocean have mostly used numerical methods.[26] Tolstoy *et al.*[27] derived an expression for the normal modes, which were approximated by Bessel functions of order $\pm 1/3$, and they conducted simulations on the long-range sound propagation at 10 Hz in the deep ocean. DiNapoli *et al.*[28] studied sound propagation in a deep-ocean sound channel across the frequency band of 1 Hz–200 Hz using the fast field program. Ryan[29] investigated the low-frequency sound field using an improved phase integral method, allowing computations with a lower frequency limit as low as 3 Hz–5 Hz in the deep ocean. Porter *et al.*[30] used a finite difference method to numerically determine the normal modes for sound propagation in a stratified ocean resting on an elastic bottom, with eigenvalues calculated at 4 Hz. Later, this method evolved into the KRAKEN model.[31] Lecoulant *et al.*[32] investigated the characteristics of VLF sound transmission in fluid–solid waveguides utilizing the SPECFEM2D program, which is based on the spectral element method; they specifically examined the VLF seismic acoustic waves that are produced by submarine earthquakes.

Under VLF conditions, having fewer normal modes leads to reduced computational complexity, making it possible to apply WKB methods to the underwater sound field. However, despite this potential, the suitability of the WKB approximation in the VLF band has not been studied extensively, and there is currently limited research on approximate methods for VLF sound propagation in the deep ocean. In response to this gap, a WKB method[33] has been introduced previously, providing an approximate solution specifically for turning modes or refracted–refracted (RR) modes, which represent eigenrays that do not reflect at the waveguide boundary. We previously expounded on the advantages of uniform asymptotic approximation in terms of parabolic cylinder function over the classical WKB method and Airy-function-based uniform asymptotic method in the calculation of very-low-frequency normal modes, but did not conduct a detailed theoretical analysis. This paper will provide a more comprehensive comparison.

Otherwise, the propagating modes in an ocean waveguide includes refracting modes and reflecting modes. At VLF, the reflecting modes may make a significant contribution at long range. Therefore, we will address the challenge of reflecting modes [such as refracted–surface–reflected (RSR) modes, refracted–bottom–reflected (RBR) modes, and surface–reflected–bottom–reflected (SRBR) modes.[34,35] By doing so, our method can be used effectively for practical computations of the VLF sound field.

The rest of this paper is arranged as follows: In Section 2 we fully describe a WKB method based on parabolic cylinder functions for calculating VLF normal modes. In Section 3 we examine the accuracy of this method across various environments, and we use it to analyze mode group velocities in typical deep-sea conditions. Finally, we conclude the paper in Section 4.

2. Normal mode theory

2.1. Fundamental solutions in a layered marine environment

For a range-independent horizontally stratified medium with a point harmonic source in a cylindrical symmetric situation, the source is at zero range and depth z_s, and the sound speed profile (SSP) in the water is denoted by $c(z)$, as shown in Fig. 1. The acoustic wave equation is written as[36]

$$\frac{\partial^2 p}{\partial r^2}+\frac{1}{r}\frac{\partial p}{\partial r}+\frac{\partial^2 p}{\partial z^2}+\frac{\omega^2}{c^2(z)}p=-\frac{2}{r}\delta(r)\,\delta(z-z_s), \quad (1)$$

where $\omega=2\pi f$ is the angular frequency and f is the source frequency. By applying the Hankel transform[7] to Eq. (1), we obtain the depth-separated wave equation, i.e.,

$$\frac{\mathrm{d}^2F(\xi,z)}{\mathrm{d}z^2}+\left[k^2(z)-\xi^2\right]F(\xi,z)=-2\delta(z-z_s),\quad 0<z<H, \quad (2)$$

where $k(z)=\omega/c(z)$ is the wavenumber at depth z. Neglecting the branch-line integral, the solution of the wave equation can be written as an infinite sum over the eigenfunctions $U_n(z)$ with eigenvalues ξ_n, i.e.,

$$p(r,z)=2\pi\mathrm{i}\sum_n U_n(\xi_n,z)\,U_n(\xi_n,z_s)\,\mathrm{H}_0^{(1)}(\xi_n r)\,\xi_n, \quad (3)$$

where $p(r,z)$ is the acoustic pressure at range r and depth z. $\mathrm{H}_0^{(1)}$ is the zeroth-order Hankel function of the first kind, and the normal mode eigenfunction is given as[37]

$$U_n(\xi_n,z)=\left.\frac{F_1(\xi,z)+(B_1/A_1)F_2(\xi,z)}{\sqrt{W(F_1,F_2)\,\dfrac{\partial}{\partial\xi}\left(\dfrac{B_1}{A_1}-\dfrac{B_2}{A_2}\right)}}\right|_{\xi_n}. \quad (4)$$

Here, $F_1(\xi,z)$ and $F_2(\xi,z)$ are the linearly independent solutions of the homogeneous counterpart of Eq. (2), H is the seawater depth. The Wronskian W, B_1/A_1, and B_2/A_2 are given

by

$$W(F_1,F_2)=F_1(\xi,z_s)F_2{}'(\xi,z_s)-F_1{}'(\xi,z_s)F_2(\xi,z_s), \quad (5)$$

$$\frac{B_1}{A_1}=-\frac{F_1(\xi,0)}{F_2(\xi,0)}, \quad (6)$$

$$\frac{B_2}{A_2}=-\frac{\mathrm{i}\gamma F_1(\xi,H)-\frac{\rho_b}{\rho_w}F_1{}'(\xi,H)}{\mathrm{i}\gamma F_2(\xi,H)-\frac{\rho_b}{\rho_w}F_2{}'(\xi,H)}, \quad (7)$$

where ρ_w is the water density and ρ_b is the bottom density, $\gamma=\sqrt{k_b^2-\xi^2}$. The eigenvalue ξ_n is the n-th root of the dispersion equation

$$\frac{B_1}{A_1}-\frac{B_2}{A_2}=0 \quad (8)$$

and such that the eigenfunction converges. If the expression for $B_1/A_1-B_2/A_2$ is too complicated for ξ to be derived easily, then we have the following alternative form of the normalized eigenfunction:[7]

$$U_n(\xi_n,z)=\left.\frac{F_1(\xi,z)+(B_1/A_1)F_2(\xi,z)}{\sqrt{\int_0^H\left[F_1(\xi,z)+\frac{B_1}{A_1}F_2(\xi,z)\right]\mathrm{d}z+\frac{F_1(\xi,z)+\frac{B_1}{A_1}F_2(\xi,z)}{2\rho_b\sqrt{\xi^2-(\omega/c_b)^2}}}}\right|_{\xi_n}. \quad (9)$$

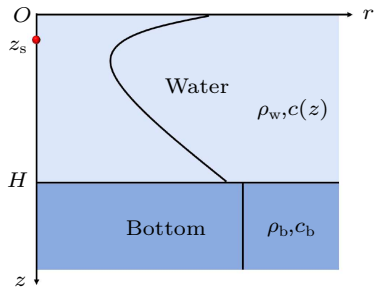


Fig. 1. Sound speed and density of layered marine environment.

2.2. Normal modes in terms of parabolic cylinder functions

The key to finding approximate solutions for normal modes is selecting the appropriate linearly independent solutions $F_1(\xi,z)$ and $F_2(\xi,z)$. As discussed in Appendix A, the reference functions method[9,36,38] or comparison equations method[39] involves assuming $q^2(z)=\left[k^2(z)-\xi^2\right]$ in Eq. (A1), $Q^2(S)=\left(E-S^2\right)$ in the mapping equation (A3), and $\chi=1$.[40] Using the properties of parabolic cylinder functions,[41] two linearly independent solutions of Eq. (2) can be expressed as

$$F_1(\xi,z)=R(E)\left(S'\right)^{-1/2}D_M(-y), \quad (10a)$$

$$F_2(\xi,z)=R(E)\left(S'\right)^{-1/2}D_M(y), \quad (10b)$$

where the function $D_M(y)$ is a parabolic cylinder function of order M (also known as the Weber function), and

$$y=\sqrt{2}S(z), \quad (11a)$$

$$E(\xi)=\frac{2}{\pi}\int_{z_1(\xi)}^{z_2(\xi)}\sqrt{k^2(z)-\xi^2}\,\mathrm{d}z, \quad (11b)$$

$$M(E)=\frac{1}{2}(E-1), \quad (11c)$$

$$R(E)=2^{1/4}\left(\frac{2e}{E}\right)^{E/4}. \quad (11d)$$

The values $z_1(\xi)$ and $z_2(\xi)$ represent the upper and lower turning points of the horizontal wavenumber ξ, respectively, and the function $S(z)$ is defined as

$$S(z):\begin{cases}\int_{s_1}^{S}\sqrt{\sigma^2-E}\,\mathrm{d}\sigma=\int_{z_1}^{z}\sqrt{\xi^2-k^2(z)}\,\mathrm{d}z, & 0<z\le z_1,\\ \int_{s_1}^{S}\sqrt{E-\sigma^2}\,\mathrm{d}\sigma=\int_{z_1}^{z}\sqrt{k^2(z)-\xi^2}\,\mathrm{d}z, & z_1<z\le z_2,\\ \int_{s_1}^{s_2}\sqrt{E-\sigma^2}\,\mathrm{d}\sigma+\int_{s_2}^{S}\sqrt{\sigma^2-E}\,\mathrm{d}\sigma=\int_{z_1}^{z_2}\sqrt{k^2(z)-\xi^2}\,\mathrm{d}z+\int_{z_2}^{z}\sqrt{\xi^2-k^2(z)}\,\mathrm{d}z, & z_2<z\le H,\end{cases} \quad (12)$$

where s_1 and s_2 are two zeros of $Q^2(S)=0$. The correspondence between S and z is shown in Fig. 2.

For the left figure in Fig. 2, when calculating turning modes, there exist turning points z_1 and z_2 such that $q^2(z)=0$ when $0<z<H$, as indicated by the solid red line. These two turning points actually exist, so we refer to them as "real turning points". For the right figure, when calculating reflecting modes such as the SRBR (surface-reflected-bottom-

reflected) modes, when $0 < z < H$, $q^2(z) > 0$, as shown by the solid red line. This means that there is no value of z for which $q^2(z) = 0$. Therefore, in order to solve for the variable E and ensure that the integral equation relationship (12) between S and z holds, we extend SSP in the negative and positive directions of the z-axis respectively, until $q^2(z)$ intersects the z-axis, as indicated by the red dotted line in the right figure. At this point, there will be z_1 and z_2 such that $q^2(z) = 0$. Since $z_1 < 0$ and $z_2 > H$, which are beyond the range of the seawater layer, they do not actually exist. Therefore, we refer to them as "virtual turning points". In this way, equation (12) between S and z also holds true when $0 \le z \le H$. $S(0)$ and $S(H)$ can be conveniently solved. By substituting these values into the dispersion equation, the eigenvalue ξ can be solved. Certainly, for RSR (refracted–surface–reflected) and RBR (refracted–bottom–reflected) modes, there are upper or lower "virtual turning points" of the horizontal wavenumber ξ.

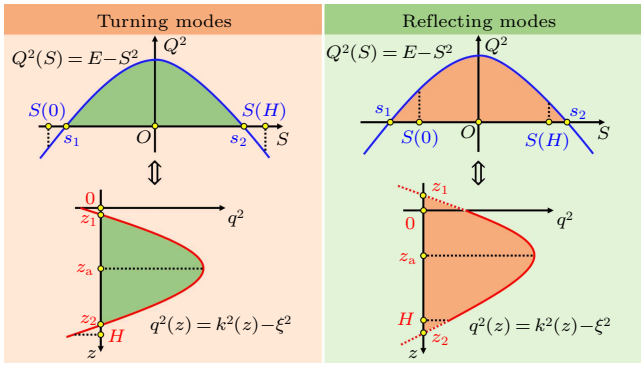


Fig. 2. Correspondence between S and z when calculating turning modes and reflecting modes (z_a denotes the depth of the channel axis).

We obtain

$$F_1'(\xi, z) = R(E)\left[\sqrt{2}D'_M(-y)\cdot(S')^{1/2} - \frac{1}{2}D_M(-y)\cdot(S')^{-3/2}\cdot S''\right], \quad (13a)$$

$$F_2'(\xi, z) = R(E)\left[\sqrt{2}D'_M(y)\cdot(S')^{1/2} - \frac{1}{2}D_M(y)\cdot(S')^{-3/2}\cdot S''\right], \quad (13b)$$

where

$$S'' = \frac{k(z)k'(z)}{\sqrt{(k^2(z)-\xi^2)(E-S^2)}} + \frac{S\left[k^2(z)-\xi^2\right]}{(E-S^2)^2}. \quad (14)$$

Hence, the dispersion equation and the eigenfunction are formulated using parabolic cylinder functions. Various numerical methods can be used to solve for the roots of the dispersion equation (8), such as bisection, the secant method, and Newton's method. We use Newton's method to find the eigenvalues, then by substituting them into Eq. (3), we obtain the WKB approximate solution for the underwater sound field based on parabolic cylinder functions.

Furthermore, from Eqs. (11b) and (11c) we obtain

$$\int_{z_1}^{z_2}\sqrt{k^2(z)-\xi_n{}^2}\,\mathrm{d}z = \left(M_n + \frac{1}{2}\right)\pi, \quad n = 0,1,2,\ldots, \quad (15)$$

which establishes a relationship between the phase integral and the order of the parabolic cylinder function, where n is the mode order. M_n is obtained by solving the dispersion equation (8) to get the eigenvalue ξ_n and then substituting it into Eq. (15), which represents the variation of the order of the parabolic cylinder function with the order of the normal mode.

Therefore, we obtain the phase shift (which relies on the upper and lower boundary conditions) for the mode as[42]

$$\delta_n = 2\left(n - M_n - \frac{1}{2}\right)\pi, \quad n = 0,1,2,\ldots. \quad (16)$$

From Eq. (16), it can be seen that the phase shift δ_n at the turning point is a function of the order M_n of the parabolic cylinder function. According to Eq. (15), the order M_n of the parabolic cylinder function is a function of frequency. Therefore, the phase shift δ_n at the turning point is also a function of frequency, and not a constant in the usual sense.

Because k, ξ, and M_n are functions of frequency,[42–44] taking the derivative of both sides of Eq. (15) with respect to ω gives

$$\frac{\mathrm{d}\xi_n}{\mathrm{d}\omega} = \frac{\displaystyle\int_{z_1}^{z_2}\left[k^2(z)-\xi_n^2\right]^{-1/2}\frac{\omega}{c^2(z)}\mathrm{d}z - \frac{\mathrm{d}M_n}{\mathrm{d}\omega}\pi}{\xi_n\displaystyle\int_{z_1}^{z_2}\left[k^2(z)-\xi_n^2\right]^{-1/2}\mathrm{d}z}, \quad (17)$$

and the reciprocal of this formula gives the group velocity as

$$v_g{}^{(n)} = \frac{\displaystyle\int_{z_1}^{z_2}\frac{\xi_n}{\sqrt{k^2(z)-\xi_n^2}}\mathrm{d}z}{\dfrac{1}{\omega}\displaystyle\int_{z_1}^{z_2}\frac{k^2(z)}{\sqrt{k^2(z)-\xi_n^2}}\mathrm{d}z - \frac{\mathrm{d}M_n}{\mathrm{d}\omega}\pi}. \quad (18)$$

Therefore, the modal group velocity can be obtained approximately without needing to integrate the eigenfunction in the depth direction.[45] According to Eq. (18), it can be seen that the group velocity $v_g{}^{(n)}$ is also a function of the order M_n of the parabolic cylinder function. Since the order M_n of the parabolic cylinder function is related to the eigenvalues, which in turn are associated with the waveguide environment being solved for, it is therefore possible to analyze the impact of changes in the waveguide environment on the group velocity.

Another important quantity in addition to the group velocity of mode n is the phase velocity, defined by

$$v_p{}^{(n)} = \frac{\omega}{\xi_n}. \quad (19)$$

2.3. Conditions for applicability of WKB method

In this subsection, we discuss qualitatively the conditions for the applicability of the approximation. According to the reference functions method (see Appendix A), these conditions can be expressed as

$$\varepsilon = \frac{1}{q^2(z)}\left[\frac{3}{4}\left(\frac{S''}{S'}\right)^2 - \frac{1}{2}\frac{S'''}{S'}\right] \ll 1, \tag{20}$$

where

$$S' = \frac{q(z)}{Q(S)}, \tag{21a}$$

$$S'' = \frac{q'(z)}{Q(S)} - \frac{Q'(S)q(z)}{Q^2(S)}\cdot S', \tag{21b}$$

$$S''' = \frac{q''(z)}{Q(S)} - \frac{Q'(S)q(z)}{Q^2(S)}\cdot S'' - \frac{2Q'(S)q(z)q'(z)}{Q^3(S)} - \frac{q^3(z)Q''(S)}{Q^4(S)} + \frac{2q^3(z)(Q'(S))^2}{Q^5(S)}. \tag{21c}$$

Moreover, from Eq. (A9), the small parameter ε represents the relative size of the right-hand side of the equation to the second term on the left-hand side, which can describe the error of the method. As a particular case, when the mapping function is chosen as $Q^2(S) = 1$, $\psi_{\text{app}}(z)$ is the classical WKB approximation and the solution to Eq. (A3) is in the form of exponential functions. From Brekhovskikh and Godin,[8] when assuming the effective refraction index $N = [\sqrt{k^2(z) - \xi^2}/k_0^2] \sim 1$, the condition can be written as

$$\varepsilon_{\text{WKB}} = \frac{1}{q^2(z)}\left\{\frac{3}{4}\left[\frac{q'(z)}{q(z)}\right]^2 - \frac{1}{2}\frac{q''(z)}{q(z)}\right\} \sim \frac{1}{k_0^2 L^2} \ll 1 \tag{22}$$

or $\lambda \ll L$, where $k_0 = \omega/c(z_0)$ is the value of $k(z)$ at reference depth $z = z_0$. L is a parameter that defines the spatial scale of the variability of the medium, and λ is the wavelength. With the choice $Q^2(S) = \pm S$, we obtain a uniform asymptotic approximation in terms of Airy functions[4,46,47] or the Langer method[48,49] for the case when $q^2(z)$ is nearly linear with a turning point.[50] Its general condition

$$\varepsilon_{\text{Airy}} = \frac{1}{q^2(z)}\left\{\frac{3}{4}\left[\frac{q'(z)}{q(z)}\right]^2 - \frac{1}{2}\frac{q''(z)}{q(z)}\right\} - \frac{5}{36}\frac{1}{\left[\int_{z_t}^{z} q(z)\,\mathrm{d}z\right]^2} \ll 1 \tag{23}$$

can be expressed as

$$\varepsilon_{\text{Airy}} \sim \frac{1}{k_0^2 L^2} - \frac{5}{36}\frac{1}{k_0^2 (z - z_t)^2} \ll 1, \tag{24}$$

where z_t is a turning point. Equations (23) and (24) are valid only when $q(z) \neq 0$ and $\int_{z_t}^{z} q(z)\,\mathrm{d}z \neq 0$, and $q'(z)$ and $q''(z)$ are not large, i.e., when z is away from z_t in a slowly varying medium.[51,52]

We have assumed $Q^2(S) = E - S^2$ in Subsection 2.2, and equation (20) will be written as

$$\varepsilon_{\text{proposed}} = \frac{1}{q^2(z)}\left\{\frac{3}{4}\left[\frac{q'(z)}{q(z)}\right]^2 - \frac{1}{2}\frac{q''(z)}{q(z)}\right\} + \left[\frac{1}{2}(E - S^2)^{-2} + \frac{5}{4}S^2(E - S^2)^{-3}\right] \ll 1. \tag{25}$$

When the upper and lower turning points $z_{1,2}$ are so close that they become a turning point of order two,[53] it is justifiable to consider E as being zero, and we obtain

$$\varepsilon_{\text{proposed}} \sim \frac{1}{[q(z)]^2}\left\{\frac{3}{4}\left[\frac{q'(z)}{q(z)}\right]^2 - \frac{1}{2}\frac{q''(z)}{q(z)}\right\} - \frac{3}{16}\frac{1}{\left[\int_{z_t}^{z} q(z)\,\mathrm{d}z\right]^2}, \tag{26}$$

which reduces to

$$\varepsilon_{\text{proposed}} \sim \frac{1}{k_0^2 L^2} - \frac{3}{16}\frac{1}{k_0^2 (z - z_t)^2} \ll 1. \tag{27}$$

Certainly, the validity of Eqs. (25)–(27) is predicated on them being the same as Eqs. (23) and (24). It can be seen from Eq. (A8) that compared to ε_{WKB}, $\varepsilon_{\text{Airy}}$, and $\varepsilon_{\text{proposed}}$ have an additional term associated with depth z under the zero-order approximation, resulting in a smaller value for ε and making it more feasible to satisfy $\varepsilon \ll 1$. Moreover, because the parameter ε improves at lower frequencies (because ε is related inversely to frequency), it is necessary to compare the accuracy of different methods in the VLF range.

3. Behavior of proposed method

3.1. Case 1: an unbounded Epstein environment

In the case of an unbounded Epstein layer, an exact solution for normal modes can be derived from the hypergeometric function,[2] and the sound speed $c(z)$ can be written as

$$c(z) = \sqrt{\frac{1}{A\operatorname{sech}^2(z/H) + B\tanh(z/H) + D}}. \tag{28}$$

For the present simulation analysis, the parameters are chosen as $A = 8.135 \times 10^{-8}$ (m/s)$^{-2}$, $B = 5.135 \times 10^{-8}$ (m/s)$^{-2}$, $D = 3.525 \times 10^{-7}$ (m/s)$^{-2}$, and $H = 4000$ m, and the SSP is as shown in Fig. 3.

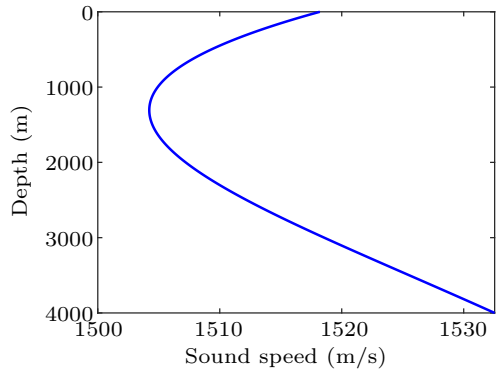


Fig. 3. Epstein sound speed profile (SSP).

In the following, we use the proposed method to calculate the normal-mode eigenvalues and eigenfunctions (see Appendix B for the solution given by this method for normal modes in the unbounded environment), and we compare them with the exact solution. Table 1 gives the results of the eigenvalue calculations for the frequencies of 5 Hz and 15 Hz.

Table 1 shows that when the frequency increases, the errors in the calculated eigenvalues decrease, and all the absolute errors are less than 10^{-6}. This means that for a distance of 1000 km, the accumulated errors of the phase in the horizontal direction are less than 1, which is negligible in comparison with the phase ξr and has little effect on the calculation of the long-distance sound field. The results of the normal-mode eigenfunction calculations for 5 Hz are shown in Fig. 4, where the eigenfunctions calculated by the proposed method agree well with the exact solutions.

Table 1. Normal-mode eigenvalues in Epstein environment.

Frequency	n	Proposed method (m^{-1})	Exact solution (m^{-1})	Error (m^{-1})
5 Hz	1	0.02083731903	0.02083764978	-3.3×10^{-7}
	2	0.02074426832	0.02074458652	-3.2×10^{-7}
15 Hz	1	0.06260737550	0.06260748710	-1.1×10^{-7}
	2	0.06251195709	0.06251206734	-1.1×10^{-7}
	3	0.06241771071	0.06241781959	-1.1×10^{-7}
	4	0.06232465393	0.06232476142	-1.1×10^{-7}
	5	0.06223280496	0.06223291102	-1.1×10^{-7}
	6	0.06214218265	0.06214228728	-1.0×10^{-7}

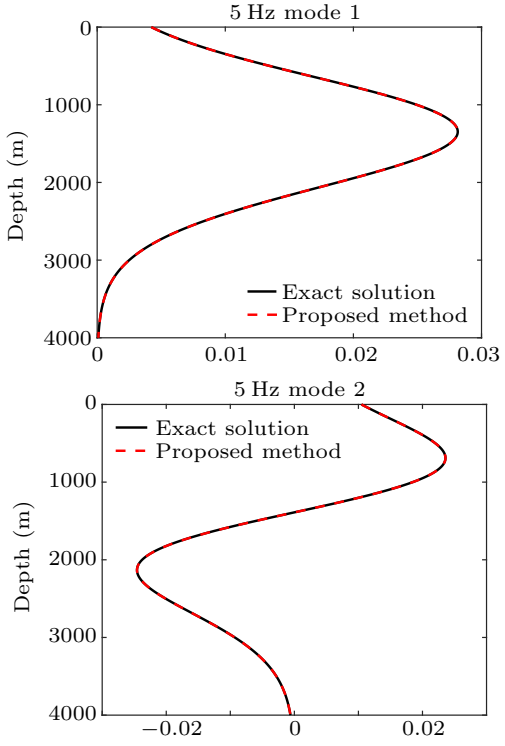


Fig. 4. Normal-mode eigenfunctions at 5 Hz: (a) mode 1, (b) mode 2.

For the sound-propagation problem discussed above, two methods are commonly used, i.e., (i) the classical WKB approximation and (ii) the uniform asymptotic approximation based on Airy functions, both of which require analytical expressions for the modes in different regions. The classical WKB approximation divides the eigenfunction into three regions,[18] but it diverges near turning points and is unsuitable for solving the sound field near these points.[13,54] The Airy-function-based uniform asymptotic approximation solves the divergence issue of the WKB approximation at the turning points, but it only applies to a single turning point. In the case of two turning points, it is necessary to match the sound field near both points[55] (see Appendix C), which affects the accuracy of the calculations[56] and is not applicable when the turning points are close together.[8,10,57] Unlike these two methods, the WKB method in terms of parabolic cylinder functions herein has the advantage that the problem does not need to be divided into regions with connection formulas, but rather a single approximate solution can be obtained that is continuous over the entire region.[58] The combination of local asymptotics may be preferable for numerical simulations, while the uniformly valid asymptotic solution is usually more convenient for analytical studies.[38]

Here, we discuss the applicability of the classical WKB approximation, the Airy-function-based uniform asymptotic approximation, and our method for computing the above problem, including the approximation conditions of the different methods and the errors in computing the transmission loss. The condition ε for each of the three methods is computed

using Eq. (20) when the frequency is 5 Hz, and the results are shown in Fig. 5.

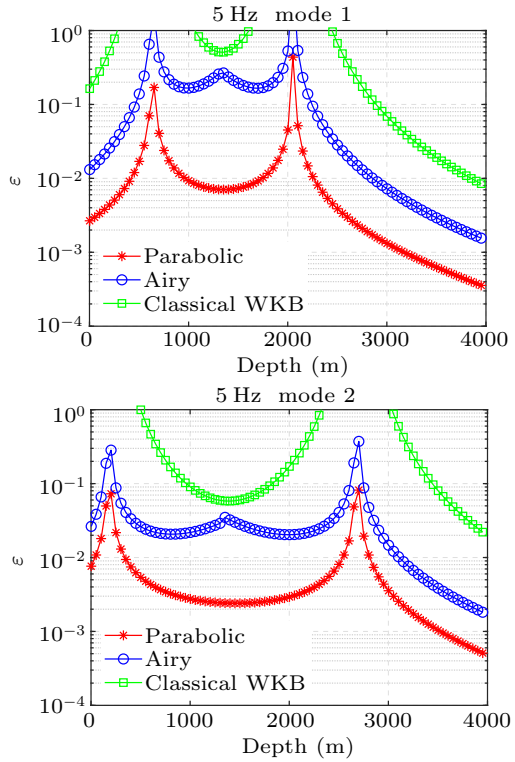


Fig. 5. Values of ε in Eq. (20) by different methods at 5 Hz: (a) mode 1, (b) mode 2. Because the formula has $q(z)$ in its denominator, ε tends to infinity for all three methods near the turning point. However, it is only the classical WKB approximate solution that actually diverges near the turning point, while the other two methods remain valid in this vicinity.

As can be seen, compared with the classical WKB approximation and the Airy-function-based uniform asymptotic approximation, our method gives very small values of ε of the order of 10^{-3}. The Airy-function-based uniform asymptotic approximation exhibits larger values of ε, particularly near the channel axis, because the nearly linear approximation fails[50] at the depths where the change in the slope of $c(z)$ is greatest.[43] Moreover, the classical WKB approximation yields even larger values of ε, reaching infinity at the turning points. Thus, it is evident that the proposed method offers the advantages of a smaller error and a broader range of depth applicability for VLF sound propagation in the deep ocean.

Next, we compare the results of the three methods regarding the transmission loss. Figure 6 shows the transmission loss and its absolute error for various sound source and receiving positions, as well as the mean absolute error for different frequencies. As can be seen, the method proposed herein results in the lowest errors; at a frequency of 5 Hz, our method gives mean errors of 0.0128 dB and 0.0096 dB, significantly smaller than the errors given by the other two methods. This improvement greatly enhances the accuracy in solving problems involving VLF sound fields. With increasing frequency, the mean errors in the calculated transmission loss decrease across all three methods. Notably, when the frequency approaches 30 Hz, the mean error of the Airy-function-based uniform asymptotic approximation converges to that of our method. The reason for this is that as the frequency increases, the error of the asymptotic approximation decreases and eventually converges to the exact solution. This trend indicates that our method excels in accurate calculations for VLF sound fields, particularly at lower frequencies.

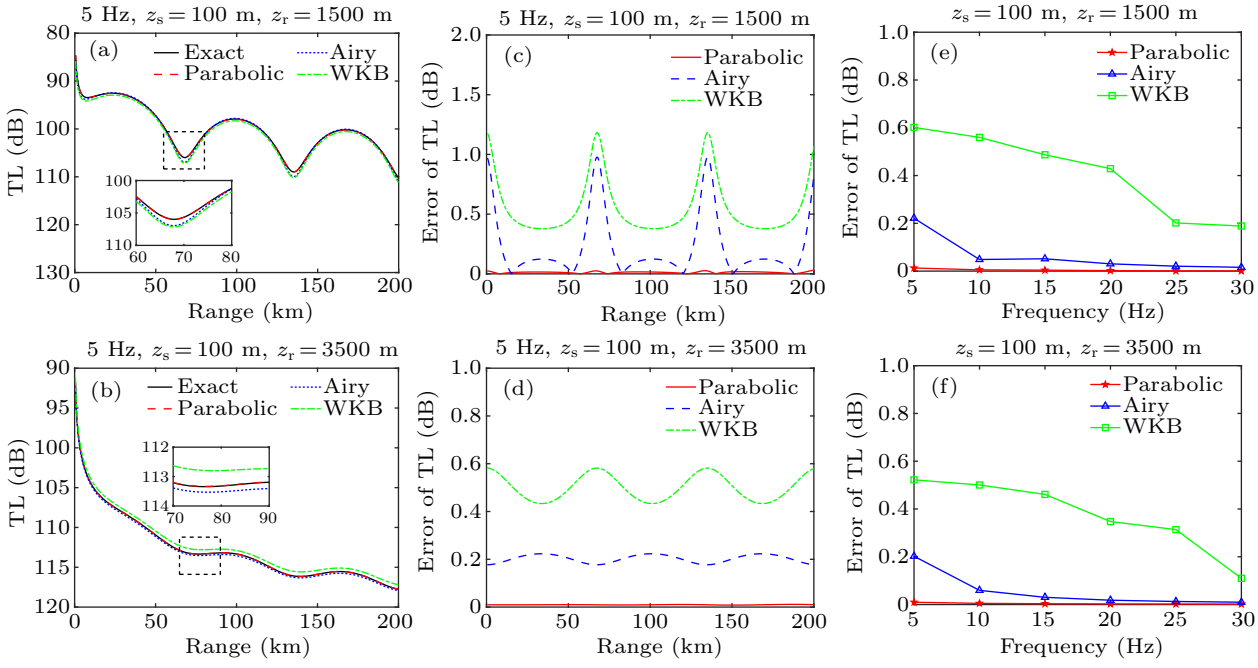


Fig. 6. Transmission loss [(a) and (b)] and its absolute error [(c) and (d)] versus range at 5 Hz for various sound source and receiving positions, and mean absolute error [(e) and (f)] at different frequencies.

3.2. Case 2: a typical Munk environment

To verify the accuracy of the proposed method in calculating the VLF sound field for a typical deep-water environment, we consider the following Munk SSP:[59]

$$c(z) = c_{\mathrm{a}}\{1+\sigma[\exp(-\eta)+\eta-1]\} \tag{29}$$

with

$$\eta = 2(z-z_{\mathrm{a}})/b, \tag{30}$$

and the parameter values are taken as $c_{\mathrm{a}} = 1478.5$ m/s, $z_{\mathrm{a}} = 800$ m, $b = 576$ m, and $\sigma = 0.003$. The water depth is 5000 m, and the bottom is assumed to be a semi-infinite fluid with $c_{\mathrm{b}} = 1800$ m/s and $\rho_{\mathrm{b}} = 1.8$ g/cm^3. The SSP is as shown in Fig. 7, where also shown is the extended SSP used to calculate the reflecting modes.

For the frequencies of 1 Hz and 8 Hz, the present method is used to calculate the eigenvalues and eigenfunctions of the turning and reflecting modes. There are four normal modes at 1 Hz and 29 normal modes at 8 Hz, and Table 2 compares the eigenvalue calculation results with those obtained using KRAKEN.[31] For these KRAKEN results, the SSP interpolation method was selected as "N2–Linear Interpolation" and RMAX was set to 1000 km, whereupon the KRAKEN results can be regarded as being "exact".[60]

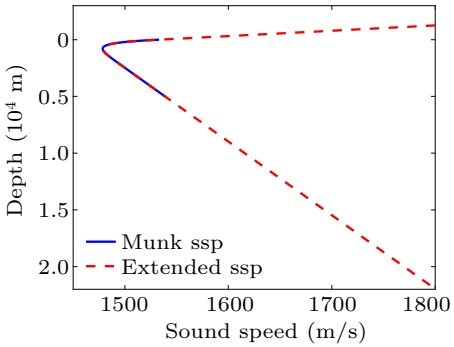


Fig. 7. Munk and extended SSPs.

Table 2. Normal-mode eigenvalues in Munk environment.

Frequency	n	Proposed method (m^{-1})	KRAKEN (m^{-1})	Error (m^{-1})
1 Hz	1	0.004156068973	0.004151599947	4.5×10^{-6}
	2	0.004024849941	0.004021925386	2.9×10^{-6}
	3	0.003828382819	0.003826999338	1.4×10^{-6}
	4	0.003535191174	0.003535454627	-2.6×10^{-7}
8 Hz	1	0.03390569021	0.03390466796	1.0×10^{-6}
	7	0.03308399897	0.03308355773	4.4×10^{-7}
	14	0.03223500369	0.03223523239	-2.3×10^{-7}
	22	0.03050639253	0.03050691450	-5.2×10^{-7}
	29	0.02819222129	0.02819268022	-4.6×10^{-7}

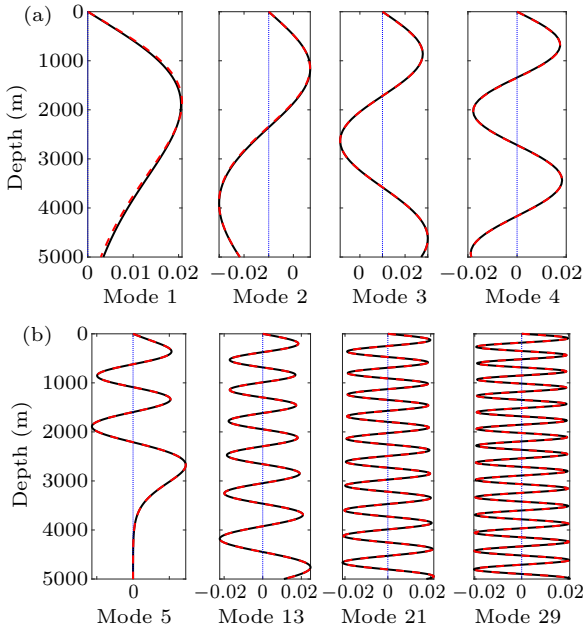


Fig. 8. Calculated results for some normal mode eigenfunctions at (a) 1 Hz and (b) 8 Hz. Black solid line: KRAKEN results. Red dashed line: results obtained using proposed method.

Table 2 shows that compared with the KRAKEN results, the errors of our eigenvalue results are less than 5×10^{-6}, even when the frequency is 1 Hz. In addition, when the frequency is increased, the errors of the eigenvalue calculation tend to decrease. Figure 8 shows the eigenfunction results calculated by our method, demonstrating consistency with the KRAKEN results.

Assuming a source depth of 300 m, the underwater sound field is calculated using the eigenvalues and eigenfunctions obtained via the proposed method, as detailed earlier. The results are then compared with those from KRAKEN, as shown in Fig. 9. As can be seen, there is generally good agreement between our method and the numerical method. The average of the absolute errors between our method and the numerical method is 0.6 dB in Fig. 9(c) and 0.3 dB in Fig. 9(f), which indicates that our solution accurately describes the VLF sound field in a typical deep ocean environment.

Next, we use Eqs. (18) and (19) for the modal group velocity and phase velocity in comparison with the KRAKEN

results. In Fig. 10, the upper curve represents the phase velocity and the lower curve represents the group velocity, and as can be seen, our method performs well. Furthermore, we use Eq. (B5) to determine the group velocity in the unbounded case. During the calculations, $\mathrm{d}M/\mathrm{d}\omega$ is less than zero and approaches zero at higher frequencies, which implies that the group velocity in this environment is lower than in an unbounded case as the frequency decreases.

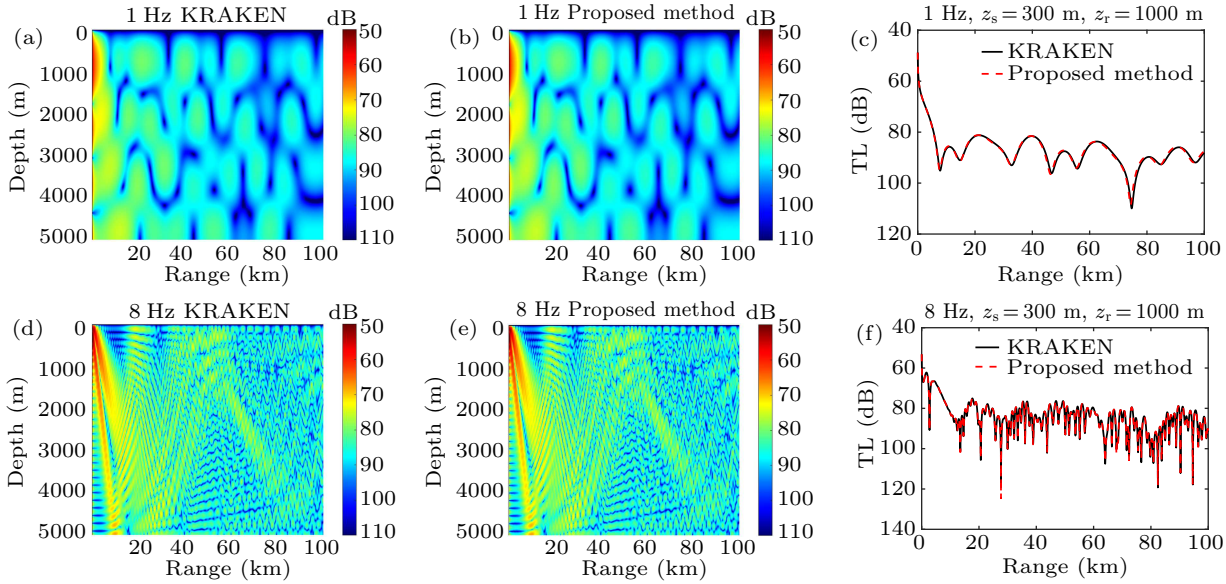


Fig. 9. Sound fields of a Munk waveguide calculated using KRAKEN [(a) and (d)], the proposed method [(b) and (e)], and curves of transmission loss versus range [(c) and (f)] for 1 Hz (top row) and 8 Hz (bottom row).

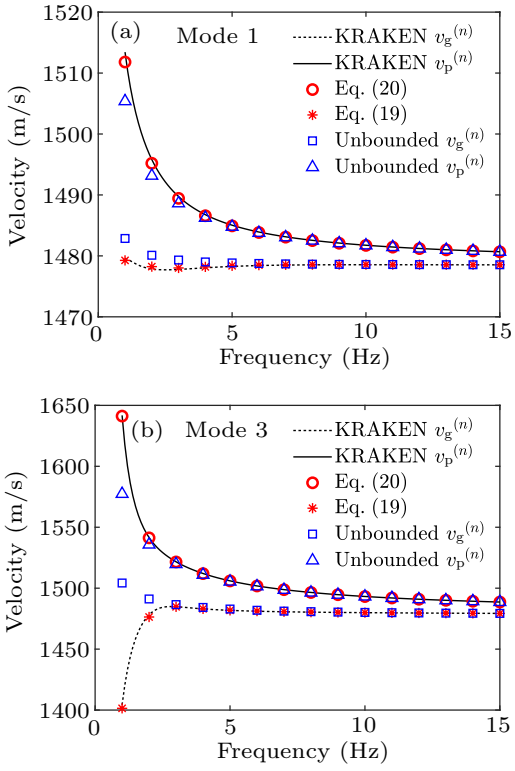


Fig. 10. Group velocity and phase velocity versus frequency: (a) mode 1, (b) mode 3.

For mode 1, we see that as the frequency decreases, the group velocity in the liquid waveguide configuration decreases gradually compared to that in the unbounded scenario. As the frequency decreases, the acoustic wavelength increases, and this causes the phase shift δ in Eq. (16) at the turning point to be notably affected by the boundary condition,[50,61,62] as indicated by the red dashed line in Fig. 11, while the phase shift is consistently $-\pi$ in the unbounded case. Consequently, there is a rise in the spacing of eigenvalues between adjacent frequencies, as depicted by the black line in the figure, leading to a reduction in the group velocity. On the other hand, for mode 3, as the frequency decreases, the grazing angle increases slightly, causing the turning mode to transform into the reflecting mode in the liquid waveguide case. This results in a decrease in the propagation distance, leading to a decrease in the group velocity.

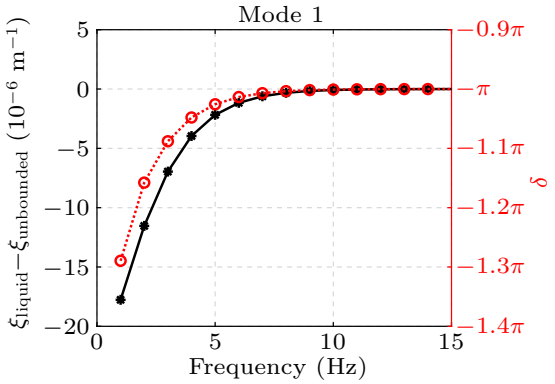


Fig. 11. Phase shift and eigenvalue difference.

Therefore, to calculate accurately the VLF sound field in the deep ocean, it is crucial to give careful consideration to the impact of the waveguide boundary; even for low-order normal modes, the changes introduced by the boundary can

significantly affect the propagation properties. Consequently, thorough modeling that considers acoustic waveguide effects is necessary for accurate predictions and analyses in the deep ocean.

Many mathematical software packages and toolboxes (e.g., Wolfram Mathematica) now offer highly efficient implementations of special functions. This makes asymptotic representations more attractive than numerically solving ordinary differential equations in many cases.[15,63] An alternative approach involves identifying appropriate asymptotic expansions for parabolic cylinder functions and representing them as elementary functions or Airy functions.[41] For instance, parabolic cylinder functions of various orders can be transformed into exponential functions. This method not only substantially reduces computational demands but also simplifies programming implementation. However, it may not be suitable for scenarios involving frequencies of a few Hertz. Consequently, we are committed to ongoing efforts to identify and develop suitable asymptotic expansions that meet our computational requirements. In our view, the WKB method based on parabolic cylinder functions is valuable in various applications.

Our method also provides some important physical sights; for example, equation (18) serves as a reliable approximation for modal group velocity in VLF ranges. From Eq. (16), M_n allows us to express the phase shift dependent on upper and lower boundary conditions, which is crucial in determining cycle distance.[41] This can be further applied to analyze underwater VLF sound propagation, especially in relation to diffraction effects that may impact source localization techniques.[64]

3.3. Case 3: a realistic incomplete channel

As illustrated in Fig. 12(a), a deep-sea sound propagation experiment was carried out in a portion of the South China Sea in July 2022 with the goal of enhancing the understanding of VLF sound propagation. Note that there are minimal fluctuations in the bathymetry along the experimental path, leading to the adoption of a range-independent model that incorporates water and seabed properties.

We present a simplified model of the ocean environment (see Fig. 12(b)) incorporating an SSP derived from averaging multiple conductivity–temperature–depth measurements. The sound channel axis is at a depth of ca. 1140 m, with a minimum sound speed of 1484 m/s. Notably, the sound speed near the ocean floor (1517.2 m/s) is lower than that of the surface seawater (1546.7 m/s), indicating an incomplete channel. Throughout the experiment, broadband explosive sources were deployed consistently at fixed depths of 100 m and 200 m, with an ocean bottom seismometer (OBS in Fig. 12(b)) serving as the receiver positioned on the seafloor.

We consider the bottom as a semi-infinite liquid with $c_\mathrm{b} = 2000$ m/s and $\rho_\mathrm{b} = 1.92$ g/cm^3 based on data from a wide-angle seismic experiment.[65] The introduction of attenuation necessitates the application of modal perturbation theory to compute complex eigenvalues.[7] We assume $\xi = \xi_\mathrm{Re} + \mathrm{i}\xi_\mathrm{Im}$, where ξ_Re is determined by the dispersion equation (8). The expression for ξ_Im can be formulated as

$$\xi_\mathrm{Im} = \xi_\mathrm{Re}^{-1} \int_0^H \frac{\alpha(z)\,\omega U^2(z)}{c(z)\,\rho(z)}\,\mathrm{d}z + \frac{U^2(H)\,\alpha_\mathrm{b}\omega}{2\xi_\mathrm{Re} c_\mathrm{b}\rho_\mathrm{b}\sqrt{\xi_\mathrm{Re}^2 - (\omega/c_\mathrm{b})^2}}, \tag{31}$$

where $\alpha(z)$ and $\rho(z)$ denote attenuation (in units Np/m) and density in the water column, respectively, and $U(z)$ denotes the normalized eigenfunction.

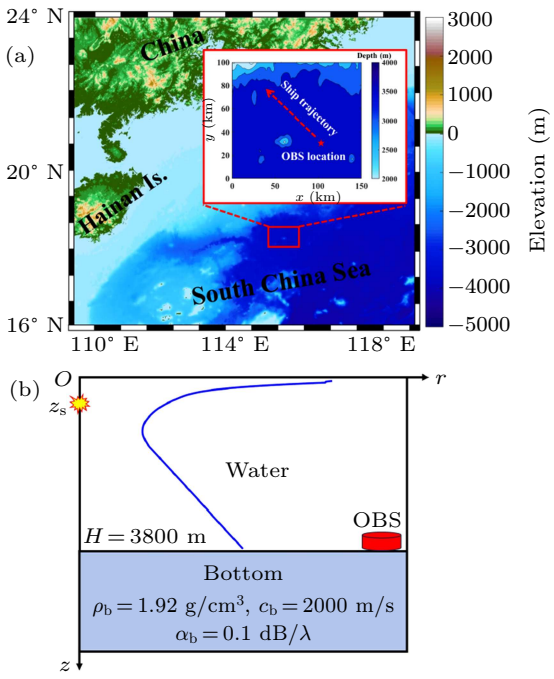


Fig. 12. Schematics of experiment: (a) water depth and ship trajectory, (b) simplified model of environment.

Given the constraints imposed by the signal-to-noise ratio of the received signals, we choose the frequency band of 8 Hz–11 Hz for computation purposes. Calculations are performed at a frequency interval of 0.1 Hz within this specified frequency band, using

$$\bar{I}(f_0) = \frac{1}{2\Delta f}\int_{f_0-\Delta f}^{f_0+\Delta f} I(f)\,\mathrm{d}f \tag{32}$$

to compute the average energy over the bandwidth.[66] To calculate the reflecting modes, we extend the measured SSP, as illustrated in Fig. 13.

The sound transmission loss for the source depths of 100 m and 200 m and the receiver depth of 3800 m is calculated using Eq. (32) and compared with that measured experimentally, as shown in Figs. 14(a) and 14(b). When only the waterborne modes and bottom bounce modes are considered for computation, the results of the proposed method align with the experimental transmission loss in the far field. However, discrepancies emerge when the source depth is 200 m and the range exceeds 70 km, resulting in the measured transmission loss being higher than the simulations because of a low signal-to-noise ratio. Furthermore, the near-field calculations yield less-satisfactory results, which constitutes a limitation of the current method. Despite these limitations, the root-mean-square errors of the transmission loss calculated by our method are 2.2 dB at a source depth of 100 m and 2.3 dB at at a source depth of 200 m when compared with the measured data, suggesting that the proposed method remains effective in predicting realistic VLF sound propagation.

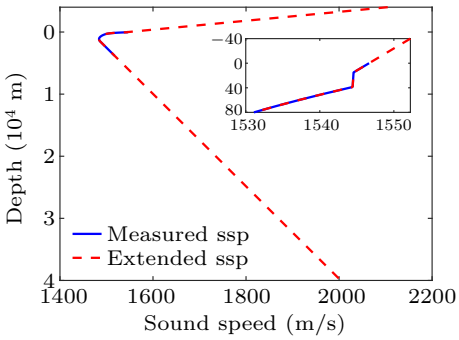


Fig. 13. Extended SSP based on measured sound speed.

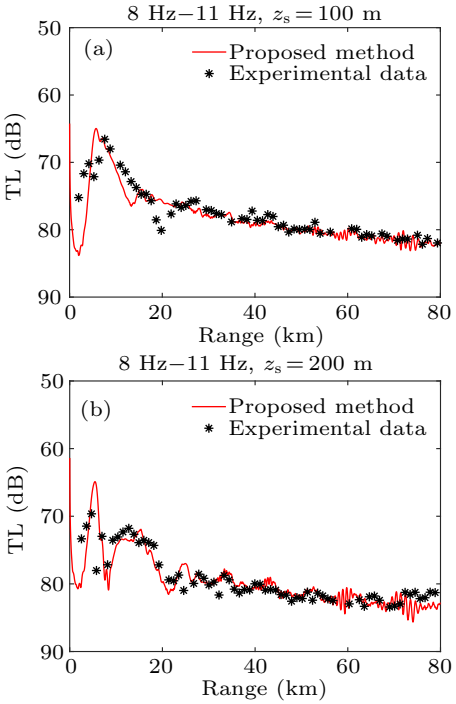


Fig. 14. Sound transmission loss for 8 Hz–11 Hz: (a) 100-m source, (b) 200-m source.

4. Conclusion

Herein, we introduced a WKB method for solving the Helmholtz equation. This method utilizes parabolic cylinder functions to express VLF normal modes in the deep ocean. It offers significant improvements over existing WKB methods in ocean acoustics, as it provides wider depth applicability and smaller errors compared to the classical WKB approximation and Airy-function-based uniform asymptotic approximation. Furthermore, we established a relationship among the phase integral, modal group velocity, and the order of the parabolic cylinder function. Our analysis reveals that even low-order normal modes can exhibit significant variations in group velocity due to boundary effects. As the frequency decreases, the group velocity in the liquid waveguide configuration decreases gradually compared to that in the unbounded scenario.

We then validated the proposed method by comparing it with the finite-difference numerical method. The transmission loss error at 1 Hz was found to be 0.6 dB. Additionally, the sound transmission loss calculated by our method aligned well with the measured data obtained from an extensive deep-sea sound propagation experiment conducted in the South China Sea.

However, the present method only considers the solution of the VLF sound field under the condition of a liquid seabed. At VLF, the sound propagation characteristics under the action of an elastic seabed are usually of concern, as well as the propagation characteristics of the interface wave and the lateral wave. This is the direction of our future efforts.

Appendix A: Reference functions method

In the reference functions method,[9,35,58] we have a second-order ordinary differential equation

$$\chi^2 \frac{\mathrm{d}^2\psi(z)}{\mathrm{d}z^2} + q^2(z)\,\psi(z) = 0, \tag{A1}$$

where χ is a small parameter. The function $\psi(z)$ has the form

$$\psi(z) = T(z)\,\phi[S(z)], \tag{A2}$$

where $\phi(z)$ is an exact solution of another second-order ordinary differential equation

$$\chi^2 \frac{\mathrm{d}^2\phi(S)}{\mathrm{d}S^2} + Q^2(S)\,\phi(S) = 0. \tag{A3}$$

The functions $Q(S)$ and $q(z)$ are qualitatively similar, and equation (A3) is called the mapping equation of Eq. (A1).

Substituting Eq. (A2) into Eq. (A1) gives the following approximate solution to Eq. (A1):

$$\psi_{\mathrm{app}} = \left(S'\right)^{-1/2}\phi(S), \tag{A4}$$

where $S(z)$ satisfies

$$\chi^2\left[\frac{3}{4}\left(\frac{S''}{S'}\right)^2-\frac{1}{2}\frac{S'''}{S'}\right]-\left(S'\right)^2Q^2+q^2=0. \tag{A5}$$

Assuming that $S(z)=S_0(z)\chi^0+S_1(z)\chi^1+S_2(z)\chi^2+\cdots$, equation (A5) can be written as

$$\begin{aligned}&\chi^0\left[-\left(S_0'\right)^4Q^2+\left(S_0'\right)^2q^2\right]+\chi^1\left[-\left(S_0'\right)^3S_1'Q^2+2S_0'S_1'q^2\right]\\&+\chi^2\left[\frac{3}{4}\left(S_0''\right)^3-\frac{1}{2}S_0'S_0'''-6\left(S_0'\right)^2\left(S_1'\right)^2Q^2\right.\\&\left.-4\left(S_0'\right)^3S_2'Q^2+\left(S_1'\right)^2q^2+2S_0'S_2'q^2\right]+\cdots=0,\end{aligned} \tag{A6}$$

so we have

$$\begin{aligned}&\chi^0:-\left(S_0'\right)^4Q^2+\left(S_0'\right)^2q^2=0,\\&\chi^1:-\left(S_0'\right)^3S_1'Q^2+2S_0'S_1'q^2=0,\\&\chi^2:\frac{3}{4}\left(S_0''\right)^3-\frac{1}{2}S_0'S_0'''-\left[6\left(S_0'\right)^2\left(S_1'\right)^2+4\left(S_0'\right)^3S_2'\right]Q^2\\&\quad+\left[\left(S_1'\right)^2+2S_0'S_2'\right]q^2=0,\\&\quad\cdots.\end{aligned} \tag{A7}$$

When all terms of order higher than χ^0 are discarded (i.e., going to zero order in χ), we obtain

$$-\left(S'\right)^2Q^2+q^2=0. \tag{A8}$$

Higher-order asymptotic approximations can be obtained by using Eqs. (A6) and (A7). The approximate solution $\psi_{\mathrm{app}}(z)$ satisfies the differential equation

$$\begin{aligned}&\chi^2\frac{\mathrm{d}^2\psi_{\mathrm{app}}(z)}{\mathrm{d}z^2}+q^2(z)\psi_{\mathrm{app}}(z)\\&=\chi^2\left[\frac{3}{4}\left(\frac{S''}{S'}\right)^2-\frac{1}{2}\frac{S'''}{S'}\right]\psi_{\mathrm{app}}(z),\end{aligned} \tag{A9}$$

and the accuracy of the approximation depends on the size of the term on the right-hand side.

Appendix B: Proposed method for unbounded case

The solution of the frequency-domain wave equation in the case of an unbounded medium can be written as[33,67]

$$p(r,z)=\begin{cases}2\pi\mathrm{i}\sum\limits_n\dfrac{F_1(\xi_n,z)F_2(\xi_n,z_{\mathrm{s}})}{\left.\dfrac{\partial W(\xi)}{\partial\xi}\right|_{\xi_n}}\mathrm{H}_0^{(1)}(\xi_n r)\xi_n, & z<z_{\mathrm{s}},\\[2ex] 2\pi\mathrm{i}\sum\limits_n\dfrac{F_1(\xi_n,z_{\mathrm{s}})F_2(\xi_n,z)}{\left.\dfrac{\partial W(\xi)}{\partial\xi}\right|_{\xi_n}}\mathrm{H}_0^{(1)}(\xi_n r)\xi_n, & z>z_{\mathrm{s}},\end{cases} \tag{B1}$$

where

$$F_1(\xi,z)=R(E)\left(S'\right)^{-1/2}D_M(-y), \tag{B2a}$$

$$F_2(\xi,z)=R(E)\left(S'\right)^{-1/2}D_M(y). \tag{B2b}$$

The parameters are defined in the same way as in Eq. (11). Using the properties of parabolic cylinder functions, the calculation yields

$$W(\xi)=-\frac{2\sqrt{\pi}R^2(E)}{\Gamma\left(\frac{1}{2}-\frac{1}{2}E\right)}, \tag{B3a}$$

$$\frac{\partial W(\xi)}{\partial\xi}=-\frac{4}{\sqrt{\pi}}R(E)T(E)\int_{z_1(\xi)}^{z_2(\xi)}\sqrt{k^2(z)-\xi^2}\,\mathrm{d}z, \tag{B3b}$$

$$T(E)=\frac{2^{1/4(-3+E)}\left(\frac{e}{E}\right)^{E/4}\ln\left(\frac{2}{E}\right)+\frac{1}{2}R(E)\Psi\left(\frac{1}{2}-\frac{1}{2}E\right)}{\Gamma\left(\frac{1}{2}-\frac{1}{2}E\right)}, \tag{B3c}$$

where $\Gamma(x)$ is the Gamma function and $\Psi(x)$ is the Digamma function,[41] and ξ_n is the nth root of the dispersion equation $W(\xi)=0$. From Eq. (B3(a)) and the nature of the zeros of the Gamma function, the dispersion equation can be simplified as

$$\int_{z_1}^{z_2}\sqrt{k^2(z)-{\xi_n}^2}\,\mathrm{d}z=\left(n+\frac{1}{2}\right)\pi,\quad n=0,1,2,\ldots \tag{B4}$$

Obviously, at this point the dispersion equation for the unbounded medium will reduce to the phase integral,[36] which has the same form as the classical WKB approximation dispersion equation. Comparing with Eq. (15), we obtain $M_n=n$ at this time. Thus, the group velocity can be expressed as

$${v_{\mathrm{g}}}^{(n)}=\frac{\displaystyle\int_{z_1}^{z_2}\frac{\xi_n}{\sqrt{k^2(z)-\xi_n^2}}\mathrm{d}z}{\dfrac{1}{\omega}\displaystyle\int_{z_1}^{z_2}\frac{k^2(z)}{\sqrt{k^2(z)-\xi_n^2}}\mathrm{d}z}. \tag{B5}$$

Appendix C: Uniform asymptotic solution based on Airy functions

For Eq. (2), we can assume a uniform asymptotic approximation in terms of Airy functions,[48,55] i.e.,

$$\varphi(\xi,z)=\begin{cases}\dfrac{1}{\sqrt{u'(z)}}\left\{C_1\mathrm{Ai}[-u(z)]+C_2\mathrm{Bi}[-u(z)]\right\}, & 0<z<z_{\mathrm{a}},\\[2ex]\dfrac{1}{\sqrt{w'(z)}}\left\{D_1\mathrm{Ai}[-w(z)]+D_2\mathrm{Bi}[-w(z)]\right\}, & z_{\mathrm{a}}<z<H,\end{cases} \tag{C1}$$

where $\varphi(\xi,z)$ denotes the unnormalized eigenfunction, z_{a} is the channel axis depth, and C_1, C_2, D_1, and D_2 are coefficients

to be determined, while $u(z)$ and $w(z)$ are expressed as

$$\begin{aligned}
&\frac{2}{3}(-u)^{3/2} = \int_z^{z_1} \sqrt{\xi^2 - k^2(z)}\,\mathrm{d}z, && z < z_1,\\
&\frac{2}{3}u^{3/2} = \int_{z_1}^{z} \sqrt{k^2(z) - \xi^2}\,\mathrm{d}z, && z > z_1,\\
&\frac{2}{3}w^{3/2} = \int_z^{z_2} \sqrt{k^2(z) - \xi^2}\,\mathrm{d}z, && z < z_2,\\
&\frac{2}{3}(-w)^{3/2} = \int_{z_2}^{z} \sqrt{\xi^2 - k^2(z)}\,\mathrm{d}z, && z > z_2.
\end{aligned} \tag{C2}$$

The condition of radiation at infinity should be considered, as the function Bi is exponentially increasing at $|z| \to \infty$, resulting in $D_1 = D_2 = 0$. When $z_1 < z < z_2$, $\varphi(\xi, z)$ should have the same asymptotic expression,[68] and from Eq. (C1) we obtain

$$\begin{aligned}
&C_1 \frac{1}{\sqrt{\pi}\sqrt{k^2(z) - \xi^2}} \sin\left(\frac{2}{3}u^{3/2} + \frac{\pi}{4}\right)\\
&= D_1 \frac{1}{\sqrt{\pi}\sqrt{k^2(z) - \xi^2}} \sin\left(\frac{2}{3}w^{3/2} + \frac{\pi}{4}\right).
\end{aligned} \tag{C3}$$

Thus we have

$$C_1 = (-1)^n D_1, \tag{C4a}$$

$$\frac{2}{3}\left(u^{3/2} + w^{3/2}\right) + \frac{\pi}{2} = (n+1)\,\pi, \quad n = 0, 1, 2\ldots. \tag{C4b}$$

From Eq. (C4b), we can also obtain the phase integral as shown by Eq. (B4). Therefore, in the unbounded case, the same dispersion equation or phase integral equation can be derived using the classical WKB approximation, the Airy-function-based uniform asymptotic approximation, and the present method.

Acknowledgements

The authors thank the team of Professor Piao Shengchun for their help with the sea experiment. Project supported by the National Natural Science Foundation of China (Grant Nos. 12174048 and 12204128).

References

[1] Pekeris C L 1948 *Geological Society of America Memoirs* **27** 1
[2] Deavenport R L 1966 *Radio Science* **1** 709
[3] Frömann N and Frömann P O 1965 *JWKB Approximation. Contributions to the Theory* (Amsterdam: North-Holland) pp. 1–9
[4] Olver F 1997 *Asymptotics and special functions* (Massachusetts: A K Peters) pp. 190–193
[5] Heading J 2013 *An introduction to phase-integral methods* (New York: Dover Publications) pp. 6–7
[6] Frisk G V 1994 *Ocean and seabed acoustics: a theory of wave propagation* (New Jersey: Pearson Education) pp. 206–209
[7] Jensen F B, Kuperman W A, Porter M B and Schmidt H 2011 *Computational ocean acoustics* (New York: Springer) pp. 143–147
[8] Brekhovskikh L M and Godin O A 2012 *Acoustics of layered media I: Plane and quasi-plane waves* (New York: Springer Science & Business Media) pp. 165–168
[9] Brekhovskikh L M and Godin O A 2013 *Acoustics of layered media II: Point sources and bounded beams* (New York: Springer Science & Business Media) pp. 201–205
[10] Berry M V and Mount K E 1972 *Rep. Prog. Phys.* **35** 315
[11] Maslov V P and Fedoriuk M V 2001 *Semi-classical approximation in quantum mechanics* (New York: Springer Science & Business Media) pp. 4–5
[12] Singh S C and Chapman C H 1988 *J. Acoust. Soc. Am.* **84** 732
[13] Godin O A 2015 *J. Fluid Mech.* **777** 260
[14] Katsnelson B G and Petrov P S 2019 *J. Acoust. Soc. Am.* **146** 1968
[15] Tsvetkova A V and Petrov P S 2023 *J. Sound Vibrat.* **548** 117555
[16] Frost B L 2024 *J. Acoust. Soc. Am.* **155** 358
[17] Wilcock W S, Stafford K M, Andrew R K and Odom R I 2014 *Annual Review of Marine Science* **6** 117
[18] Budden K 1961 *The Wave-guide Mode Theory of Wave Propagation* (London: Logos Press) pp. 196–200
[19] Henrick R, Brannan J, Warner D and Forney G 1983 *J. Acoust. Soc. Am.* **74** 1464
[20] Zhang R H and He Y 1995 *J. Sound Vibrat.* **179** 313
[21] Ainslie M A, Packman M N and Harrison C H 1998 *J. Acoust. Soc. Am.* **103** 1804
[22] Aksenov S and Kuznetsov G 2021 *Acoust. Phys.* **67** 474
[23] Guthrie K 1974 *J. Sound Vibrat.* **32** 289
[24] Beilis A 1983 *J. Acoust. Soc. Am.* **74** 171
[25] Leibiger G A 1968 *Wave propagation in an inhomogeneous medium with slow spatial variation*, Ph. D. Dissertation (New Jersey: Stevens Institute of Technology)
[26] Tango G J 1988 *IEEE Journal of Oceanic Engineering* **13** 198
[27] Tolstoy I and May J 1960 *J. Acoust. Soc. Am.* **32** 655
[28] DiNapoli F, Powers M and Browning D 1973 *J. Acoust. Soc. Am.* **53** 299
[29] Ryan F 1978 *J. Acoust. Soc. Am.* **64** S24
[30] Porter M B and Reiss E L 1984 *J. Acoust. Soc. Am.* **76** 244
[31] Porter M B 1991 *The KRAKEN normal mode program* (Washington D.C.: Naval Research Laboratory) pp. 1–202
[32] Lecoulant J, Guennou C, Guillon L and Royer J Y 2022 *J. Acoust. Soc. Am.* **151** 3437
[33] Piao S C and Zhan J K 2024 *Acta Acustica* **49** 784 (in Chinese)
[34] Song W H, Wang N, Gao D Z, Wang H Z, Hu T and Guo S M 2017 *J. Acoust. Soc. Am.* **142** 1848
[35] Brown M G 2020 *J. Acoust. Soc. Am.* **147** 898
[36] Brekhovskikh L M 1960 *Waves in layered media* (New York: Academic Press) pp. 171–172
[37] Wang D Z and Shang E C 1981 *Underwater Acoustics*, 2nd edn. (Beijing: Sci. Press) pp. 63–66 (in Chinese)
[38] Godin O A 2016 *J. Acoust. Soc. Am.* **140** 283
[39] Dingle R 1956 *Appl. Sci. Res., Section B* **5** 345
[40] Fröman N and Fröman P O 1998 *Phase-integral method: allowing nearlying transition points* (New York: Springer-Verlag) pp. 15–17
[41] Abramowitz M and Stegun I A 1964 *Handbook of mathematical functions with formulas, graphs, and mathematical tables* (Washington: U.S. Govt. Print. Off.) pp. 685–700
[42] Harrison C H 2012 *J. Acoust. Soc. Am.* **132** 48
[43] Mitchell S K 1976 *An extension of Langer's asymptotic solution with applications to ocean acoustics*, Ph. D. Dissertation (Texas: The University of Texas at Austin)
[44] Niu H Q, Zhang R H and Li Z L 2014 *J. Acoust. Soc. Am.* **136** 53
[45] Koch R A, Penland C, Vidmar P J and Hawker K E 1983 *J. Acoust. Soc. Am.* **73** 820
[46] Erdélyi A 1960 *J. Math. Phys.* **1** 16
[47] Wasow W 2012 *Linear turning point theory* (New York: Springer Science & Business Media) pp. 3–5
[48] Langer R E 1937 *Phys. Rev.* **51** 669
[49] Langer R E 1949 *Trans. Am. Math. Soc.* **67** 461
[50] Murphy E and Davis J 1974 *J. Acous. Soc. Am.* **56** 1747
[51] Langer R E 1950 *Commun. Pure Appl. Math.* **3** 427
[52] Kawahara H 1984 *Asymptotic analysis of ocean bottom reflected acoustic fields*, Ph. D. Dissertation (Massachusetts: Massachusetts Institute of Technology and Woods Hole Oceanographic Institution)
[53] Lynn R Y S and Keller J B 1970 *Commun. Pure Appl. Math.* **23** 379
[54] Zhang R H and Wang Q 1990 *J. Acoust. Soc. Am.* **87** 633
[55] Miller W H 1968 *J. Chem. Phys.* **48** 464
[56] Pack R T 1972 *J. Chem. Phys.* **57** 4612
[57] Ahluwalia D S and Keller J B 2005 *Wave Propagation and Underwater Acoustics* (New York: Springer-Verlag) pp. 14–85
[58] Miller S C and Good R 1953 *Phys. Rev.* **91** 174
[59] Munk W H 1974 *J. Acoust. Soc. Am.* **55** 220

[60] Levinson S J, Westwood E K, Koch R A, Mitchell S K and Sheppard C V 1995 *J. Acoust. Soc. Am.* **97** 1576
[61] Toyohiko Ishihara T I and Kouji Ohshima K O 1993 *Jpn. J. Appl. Phys.* **32** 2483
[62] Feng X and Gar Lam Y 1994 *Journal of Lightwave Technology* **12** 443
[63] Anikin A Y, Dobrokhotov S Y, Nazaikinskii V E and Tsvetkova A V 2019 *Theor. Math. Phys.* **201** 1742
[64] Worthmann B M and Dowling D R 2020 *J. Acoust. Soc. Am.* **147** 3959
[65] Wu Z L, Li J B, Ruan A G, Lou H, Ding W W, Niu X W and Li X B 2012 *Sci. China-Earth Sci.* **55** 159
[66] Chen Y C, Zhang M H and Gong L J 2023 *JASA Express Letters* **3** 096001
[67] Bucker H P 1970 *J. Acoust. Soc. Am.* **48** 1187
[68] Bender C M and Orszag S A 1999 *Advanced mathematical methods for scientists and engineers I: Asymptotic methods and perturbation theory* (New York: Springer Science & Business Media) pp. 519–520